Enhanced Chaos Generation in Mid-Infrared Interband Cascade Lasers Under Amplitude-Modulated Optical Injection

Han, Hong; Xu, Jiada; Jia, Zhiwei; Zhang, Jianguo; Huo, Mingming ; Shore, K. Alan

Photonics

DOI:
10.3390/ photonics11121192

Published: 19/12/2024

Publisher's PDF, also known as Version of record

photonics

MDPI

Article

Enhanced Chaos Generation in Mid-Infrared Interband Cascade Lasers Under Amplitude-Modulated Optical Injection

Hong Han [1,*], Jiada Xu [1], Zhiwei Jia [1], Jianguo Zhang [1], Mingming Huo [2] and K. Alan Shore [3]

[1] Key Laboratory of Advanced Transducers and Intelligent Control System, Ministry of Education, College of Physics and Optoelectronics, Taiyuan University of Technology, Taiyuan 030024, China
[2] Qingdao Branch, Naval Aeronautical University, Qingdao, 266041, China
[3] School of Computer Science and Electronic Engineering, Bangor University, Wales LL57 1UT, UK
* Correspondence: hanhong@tyut.edu.cn

Abstract: We numerically investigate the dynamics of an interband cascade laser (ICL) subjected to amplitude-modulated optical injection from a directly modulated master ICL. In comparison with steady-state optical injection, the proposed modulated optical injection significantly enlarges the chaos region. In excess of 10 GHz broadband mid-infrared chaos is obtained at large bias currents and with a high gain stage number for the appropriate choice of master-slave detuning, modulation frequency, and modulation depth.

Keywords: mid-infrared chaos; interband cascade laser; amplitude-modulated optical injection

Received: 19 November 2024
Revised: 17 December 2024
Accepted: 18 December 2024
Published: 19 December 2024

Citation: Han, H.; Xu, J.; Jia, Z.; Zhang, J.; Huo, M.; Shore, K.A. Enhanced Chaos Generation in Mid-Infrared Interband Cascade Lasers Under Amplitude-Modulated Optical Injection. *Photonics* **2024**, *11*, 1192. https://doi.org/10.3390/photonics11121192

1. Introduction

It is appreciated that the mid-infrared regime (3–5 μm and 8–12 μm) has low-loss free-space transmission [1,2]. Chaos is a general physical phenomenon in which noise-like waveforms are described by deterministic equations without stochastic terms [3]. A key signature of optical chaos is the appearance of broadband optical spectra. In consequence, mid-infrared optical chaos is of interest for secure optical communications and anti-jamming lidar in free space [4–7]. As such, the generation of mid-infrared chaos has been the focus of recent research efforts. Optical feedback, optoelectronic feedback, and optical injection are three typical external perturbations that have been thoroughly explored for chaos generation in the near-infrared regime [8–10]. Attention has been given to mid-infrared devices, such as quantum cascade lasers (QCLs) and interband cascade lasers (ICLs). A mid-infrared chaotic low-frequency fluctuation was observed experimentally in a QCL with optical feedback [11,12]. Although there is no relaxation frequency oscillation in a QCL, it is difficult to obtain broadband strong chaos due to its ultra-short carrier lifetime (around 0.1 ps) and the small value of the linewidth bandening factor–less than 0.5 [12]. QCLs under optical injection produced both periodic oscillations and spiking pulsations rather than chaos [13,14]. As a type-II quantum well interband transition emission laser, ICL possesses a sub-nanosecond order carrier lifetime similar to that of regular class-B semiconductor lasers [15]. It also has some unique features, such as a linewidth broadening factor of 1.1 to 2.2, and cascading gain stage numbers of 5 to 20 [16]. ICLs subject to optical feedback have been investigated theoretically [17] and in experiments [18,19] where a 6 GHz bandwidth chaos has been observed quite recently [19]. Optoelectronic feedback is sensitive to the feedback phase. However, only continuous periodical

oscillation, low-frequency regular pulses, and intermittent oscillations were observed in experiments where the ICL was subjected to optoelectronic feedback [20]. More recently, 318 MHz mid-infrared chaos was found in ICL subjected to optical injection [21]. However, this chaos regime is restricted to near-threshold pump currents and some values of frequency detuning between the master (transmitter) laser and the slave (receiver) laser, and generally the slave laser operates in a period-1 oscillatory state or a stable locking regime. It should be noted that the above-mentioned optical injection has a fixed intensity. In comparison with fixed intensity optical injection, amplitude-modulated optical injection with an appropriate modulation depth and modulation frequency would be expected to give rise to more complex nonlinear dynamics of the slave laser. Modulated optical injection has been applied to conventional distributed feedback (DFB) lasers, in which the injection strength is modulated, resulting in broad-bandwidth chaos for appropriate modulation parameters [22,23]. Such external amplitude-modulated optical injection has also been explored in vertical-cavity surface-emitting lasers (VCSELs) where over 40 GHz bandwidth chaos was obtained [24].

In this paper, we numerically study the dynamics of an ICL subject to amplitude-modulated optical injection. Here, it is assumed that the master ICL is directly modulated to provide amplitude-modulated optical injection into the slave ICL. The dynamics of such a slave ICL under both steady-state and modulated optical injection are investigated. It is found that the region of chaos associated with modulated optical injection is significantly enlarged compared with that obtained with steady-state optical injection. The stable locking state for steady-state optical injection is replaced by periodic oscillations when the slave laser is subject to amplitude-modulated optical injection. In addition, large bias currents enable broadband chaos generation in amplitude-modulated optical injection. In combination with a large number of ICL gain stages, the bandwidth of mid-infrared chaos is further enhanced.

2. Model for Simulations

Figure 1 shows the proposed experimental arrangement, which is simulated here. A sinusoidal waveform generator (SWG) is used to generate a GHz order sinusoidal wave, which is added to the bias current of the master ICL to obtain amplitude-modulated optical injection. The output light of the master ICL is collimated by an aspheric lens, and then a polarization-dependent isolator is used to inject it unidirectionally into the slave ICL. Between the isolator and the collimating lens, a half-wave plate is used to adjust the injection strength by changing the direction of the linear polarization. The light is divided into two branches using a beam splitter. One branch is injected into the slave ICL, and the other branch is used to monitor the master ICL's injection power using a power meter.

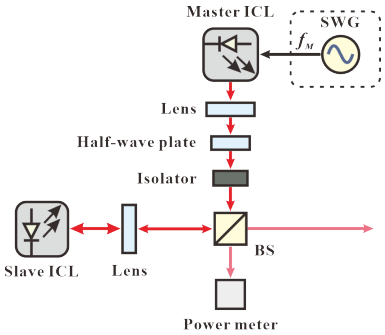

Figure 1. Schematic diagram of ICL subjected to modulated optical injection. SWG: sinusoidal waveform generator, BM: beam splitter.

In the simulations, modified Lang-Kobayashi rate equations are used in refs. [17,21,25,26]. The dynamics of the slave ICL with optical injection are prescribed by Equations (1)–(3), where $N_s(t)$ is the carrier number of the slave laser, $S_s(t)$ is the photon number of the slave laser, and $\phi_s(t)$ is the phase difference between the slave laser and the master laser.

$$\frac{dN_s(t)}{dt} = \eta\frac{I_s}{q} - \Gamma_p v_g g S_s(t) - \frac{N_s(t)}{\tau_{sp}} - \frac{N_s(t)}{\tau_{aug}} \tag{1}$$

$$\frac{dS_s(t)}{dt} = \left(m\Gamma_p v_g g - \frac{1}{\tau_p}\right)S_s(t) + m\beta\frac{N_s(t)}{\tau_{sp}} + 2k_i\sqrt{S_s(t)S_m(t-\tau_i)}\cos\phi \tag{2}$$

$$\frac{d\phi_s(t)}{dt} = \frac{\alpha_H}{2}\left(m\Gamma_p v_g g - \frac{1}{\tau_p}\right) - k_i\sqrt{\frac{S_m(t-\tau_i)}{S_s(t)}}\sin\phi \tag{3}$$

where η is the current injection efficiency, I_s is the pump current of the slave laser, Γ_p is the optical confinement factor per gain stage, v_g is the group velocity of light, and g is the material gain per stage, which is given by $g = a_0[N(t) - N_{tr}]/A$. a_0 is differential gain and A is the active area which is given by $A = W \times L$. τ_{sp} is the spontaneous radiation lifetime, and τ_{aug} is the Auger recombination lifetime. m is the number of the cascade gain stage, τ_p is the photon lifetime. τ_i is the external injection time, and $k_i = 2C_l\sqrt{r_{inj}}/\tau_{in}$ is the injection efficiency, which is defined as the power ratio between the injection light and the laser output, where τ_{in} is the internal cavity round trip time, and C_l is an external coupling coefficient that can be expressed as $C_l = (1 - R)/2\sqrt{R}$, with R is the facet reflectivity. β is the spontaneous emission factor, and α_H is the linewidth broadening factor. Δf is the frequency detuning between the master and the slave laser. The relaxation frequency oscillation can be expressed as follows: $f_R = \sqrt{(\Gamma_p v_g a_0 S_s)/(A\tau_p)}/(2\pi)$. The threshold current is $I_{th} = (q/\eta)(A/(m\Gamma_p v_g a_0\tau_p) + N_{tr})(1/\tau_{sp} + 1/\tau_{aug})$, and the value of the threshold current is 17.6 mA. In modulated optical injection, the pump current of the master laser is $I_m = I_m + h(I_m - I_{th})\sin(2\pi f_M t)$, where f_M is the modulation frequency, and h is the modulation depth [27]. In this way, the bias current of the master laser is modulated, and the maximum modulation depth should be less than unity to ensure that the master laser is always on so as to provide continuous optical injection into the slave laser. Table 1 provides the detailed parameters of the ICL used in the simulation. Except where indicated otherwise, the gain stage number of the ICL is 10.

Table 1. ICL parameters used in the simulation.

Symbol	Description	Values
L	Cavity length	2 mm [28]
W	Cavity width	4.4 μm [28]
A	Active area	8.8×10^{-9} m^2
R	Facet reflectivity	0.32 [15]
n_r	Refractive index	3.58 [15]
Γ_p	Optical confinement factor	0.04 [15]
η	Injection efficiency	0.64 [29]
τ_p	Photon lifetime	10.5 ps
τ_{sp}	Spontaneous emission lifetime	15 ns [29]
τ_{aug}	Auger lifetime	1.08 ns [29]
I_{th}	Threshold current	17.6 mA
a_0	Differential gain	2.8×10^{-10} cm [30]

N_{tr}	Transparent carrier number	6.2×10^7 [30]
β	Spontaneous emission factor	1×10^{-4} [31]
α_H	α factor	2.2 [16]
m	Gain stage number	10~17
τ_i	Injection time delay	2 ns
r_{inj}	Injection strength	−20 dB~0 dB
k_i	Coupling coefficient	2.52×10^9~2.52×10^{10}/s
Δf	Frequency detuning	−6 GHz~6 GHz
f_M	Modulation frequency	2 GHz/2.5 GHz/4 GHz~10 GHz
h	Modulation depth	0~0.85

Figure 2 presents the modulation response of the master ICL. As expected, the peak of the modulation response curves moves to a high frequency as the bias current rises: the peak at 1.90 GHz moves to 5.85 GHz and the 3 dB bandwidth at 1.53–2.25 GHz rises to 2.63–7.89 GHz when the bias current increases from $1.2I_{th}$ to $3I_{th}$. When the bias current is further increased to $4I_{th}$, the 3 dB bandwidth becomes 9.95 GHz.

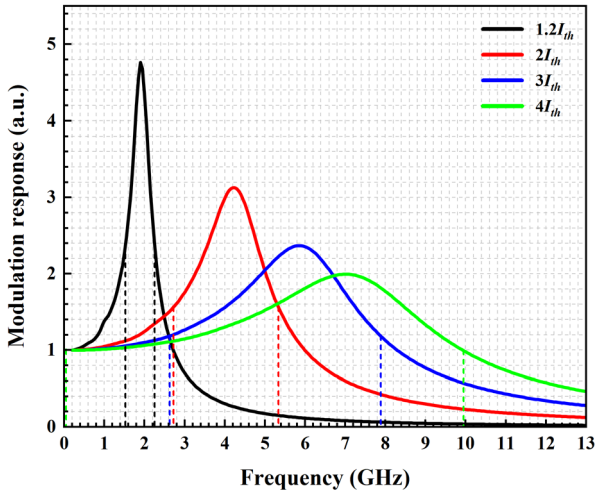

Figure 2. Modulation response curves of the master laser. Black, red, blue and green curves respectively present bias current of ICL at $1.2I_{th}$, $2I_{th}$, $3I_{th}$, and $4I_{th}$. The corresponding 3 dB bandwidths are marked by black, red, blue, and green dashed lines, respectively.

3. Results

3.1. Steady-State Optical Injection

With steady-state optical injection, that is, the modulation depth is zero, the output of the slave laser exhibits a range of dynamical behaviors, including stable locking, period-1, period-2, quasi-periodic, and chaos in a relatively low bias current, that is, $1.2I_{th}$, where the detuning frequency and injection ratio respectively range from −6 GHz to 6 GHz and −20 dB to 0 dB. The corresponding map of the dynamics is shown in Figure 3a; chaos (red region) appears in a very narrow, scattered region. Even with relatively high values of the ICL bias current, here it is $2I_{th}$, and no chaos appears, as shown in Figure 3b. These results are in accordance with those of ref. [21]. The absence of chaos can be attributed to the large damping factor at increasing bias currents [21,32].

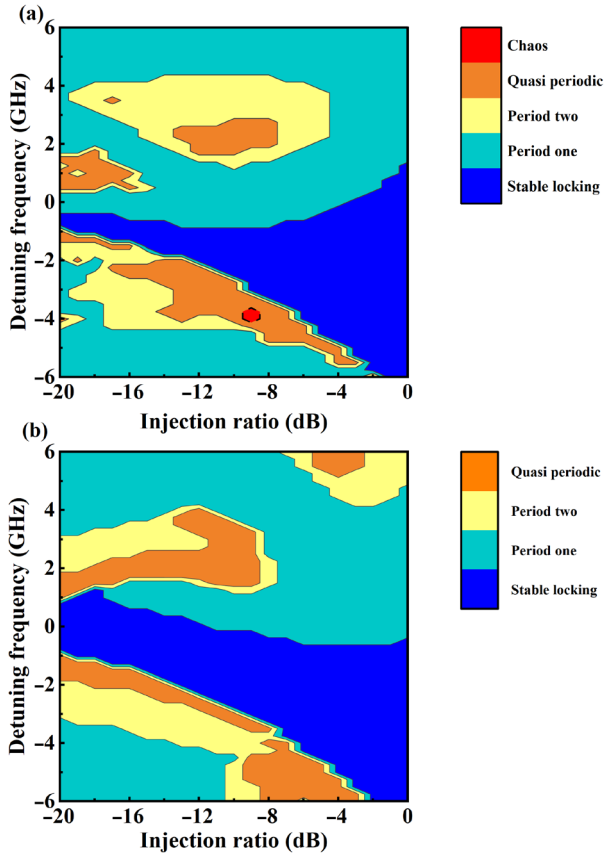

Figure 3. Detuning versus injection strength map of the nonlinear dynamics of the ICL with stable optical injection in terms of the modulation. The bias currents of the master and slave lasers are $1.2I_{th}$ for (**a**) and $2I_{th}$ for (**b**).

Figure 4 shows a time series of period-1 at detuning frequencies of 1 GHz (Figure 4a), 4.5 GHz (Figure 4b), and −6 GHz(Figure 4c). It is found that the frequency span of period-1 in Figure 4a is around 2.61 GHz, which is a little larger than the relaxation oscillation frequency of the slave laser biased at $1.2I_{th}$. For the relatively high detuning frequency of 4.5 GHz, the frequency span of period-1 is 4.7 GHz, as shown in Figure 4b. With a detuning frequency of −6 GHz, the frequency span of period-1 is 6.09 GHz, as presented in Figure 4c. These results illustrate that for steady-state optical injection, the detuning frequency plays a key role in determining the frequency span of period-1 oscillations. In addition, the peak-to-peak photon number decreases as the magnitude of the detuning frequency increases, so that its value is 2.0 for 1 GHz detuning and 1.2 for 4.5 GHz detuning, and is 0.9 for −6 GHz detuning.

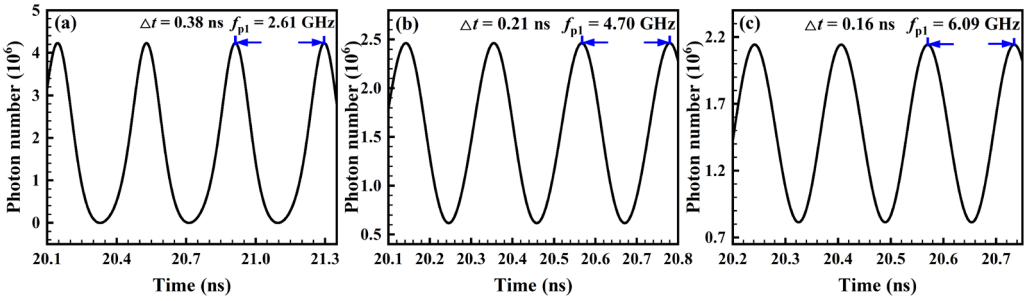

Figure 4. Temporal waveforms for different detuning frequencies: (**a**) $\Delta f = 1$ GHz, (**b**) $\Delta f = 4.5$ GHz, and (**c**) $\Delta f = -6$ GHz. The injection ratio is fixed at −10 dB. The bias currents of master and slave lasers in the simulation are $1.2I_{th}$.

3.2. Modulated Optical Injection

For modulated optical injection, the modulation depth and the modulation frequency are key control parameters. Considering the modulation response of the ICL, the modulation frequency here is initially set at 2.5 GHz when the bias current is $1.2I_{th}$. It is found that modulated optical injection gives rise to the output of the slave laser, which is not simply period-1. At a very small modulation depth of 0.01, the output of the slave laser is period-1, as Figure 5a shows. As the modulation depth increases to 0.1, and then to 0.6, quasi-periodic and chaotic behaviors successively occur, as shown respectively in Figure 5b and Figure 5c.

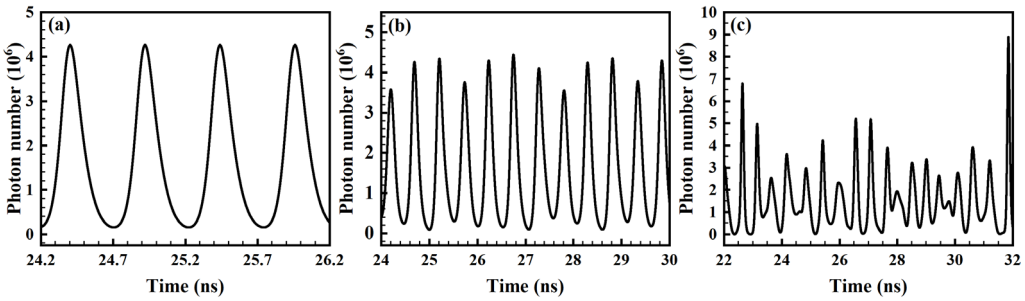

Figure 5. Temporal waveforms for different modulation depths: (**a**) h = 0.01, (**b**) h = 0.1, and (**c**) h = 0.6. The injection ratio is fixed at −17 dB, and the detuning frequency is 0.25 GHz. The bias currents of master and slave lasers in the simulation are $1.2I_{th}$.

Apart from changes in period-1 dynamics, with increasing modulation depth, the stable locking found for steady-state optical injection (h = 0, Figure 6a) is replaced by period-1 dynamics, quasi-periodic dynamics, and chaos, as shown in Figure 6b–d. The frequency span of period-1 for modulated optical injection is determined by the modulation frequency; in Figure 6b, arrows indicate that the corresponding frequency span is 2.5 GHz.

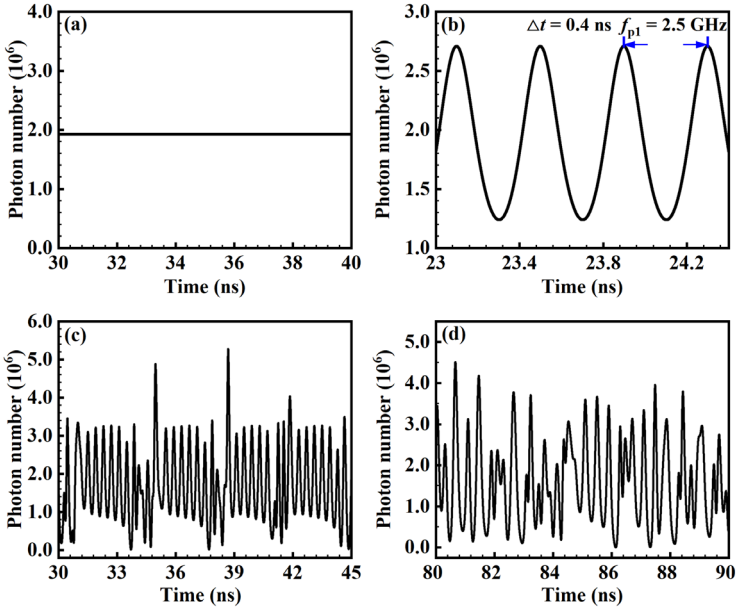

Figure 6. Temporal waveforms for different modulation depths: (**a**) h = 0, (**b**) h = 0.3, (**c**) h = 0.5, and (**d**) h = 0.65. The modulation frequency is 2.5 GHz, the injection ratio is fixed at −9 dB, and the detuning frequency is −3 GHz. The bias currents of the master lasers and slave lasers in the simulation are $1.2I_{th}$.

An overview of the nonlinear dynamics of the slave laser with modulated optical injection as a function of the frequency detuning and injection ratio is shown in Figure 7. As expected, the chaos region is significantly enlarged due to the modulated optical injection, especially at negative detuning frequencies. The stable locking state found for steady-state optical injection is replaced by period-1, period-2, and quasi-periodic dynamics. In Figure 7a, the modulation depth is 0.3. It is confirmed that with a relatively large modulation depth, the region of chaos is further enlarged, as presented in Figure 7b, where the modulation depth is 0.65.

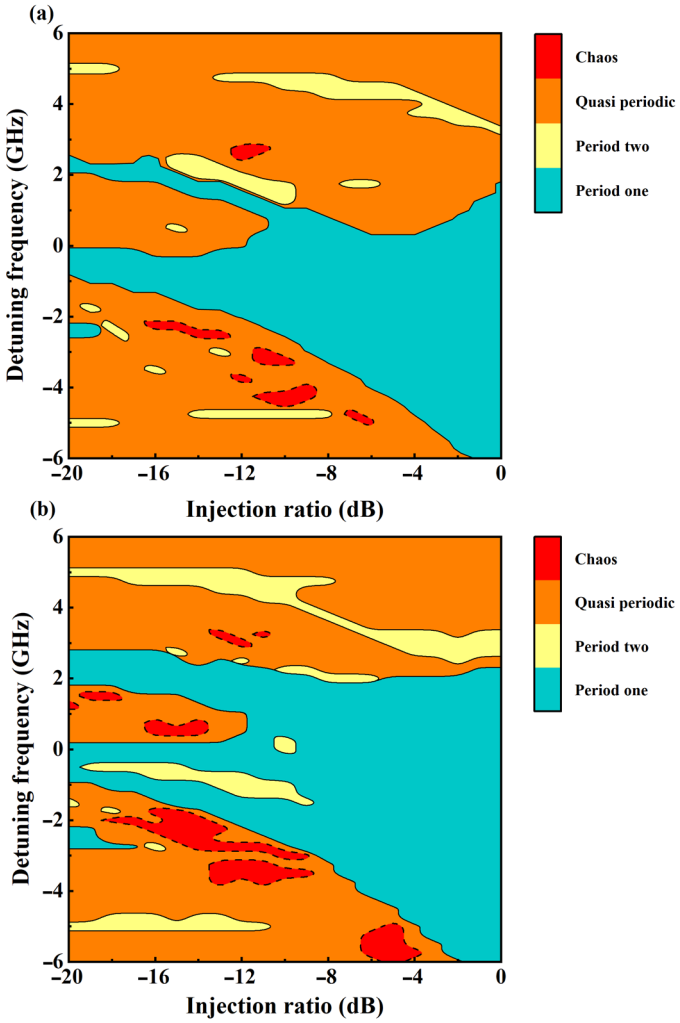

Figure 7. Detuning versus injection strength map of the nonlinear dynamics of the slave ICL with modulated optical injection. The bias currents of master and slave lasers in the simulation are $1.2I_{th}$. The modulation frequency and the modulation depth of the master laser are set as 2.5 GHz and 0.3 for (**a**) and 0.65 for (**b**).

Figure 8 presents the time series (Figure 8a), the radio frequency (RF) spectrum (Figure 8b), the autocorrelation function (Figure 8c), and the maximum Lyapunov exponent (Figure 8d) of chaos where the detuning frequency is −5.75 GHz, and the modulation frequency is 2.5 GHz. We use the traditional definition of bandwidth of chaos, that is, 80% power bandwidth [6,10,19,23,24,33]. The bandwidth of chaos is 4.26 GHz, as marked with the blue dashed line in Figure 8b. The autocorrelation function $A(\Delta t)$, which is used to quantify the chaos synchronization quality, is defined as [4,8,17,23]

$$A(\Delta t)=\frac{\left\langle \left(S_s(t+\Delta t)-\left\langle S_s(t+\Delta t)\right\rangle\right)\cdot\left(S_s(t)-\left\langle S_s(t)\right\rangle\right)\right\rangle}{\sqrt{\left\langle \left(S_s(t+\Delta t)-\left\langle S_s(t+\Delta t)\right\rangle\right)^2\right\rangle\cdot\left\langle \left(S_s(t)-\left\langle S_s(t)\right\rangle\right)^2\right\rangle}} \quad (4)$$

where $S_s(t+\Delta t)$ contains the time shift Δt with respect to $S_s(t)$, and $\langle\cdot\rangle$ stands for time averaging. Since there are multiple peaks in the autocorrelation function, as presented in Figure 8c, it is difficult to obtain the injection time delay. The largest Lyapunov exponent λ is the slope of the blue line shown in Figure 8d, $\lambda = (\ln(d(t)) - \ln(d(0)))/t$ [34]. The value of λ is larger than zero, indicating that the outputs of the ICL are chaotic.

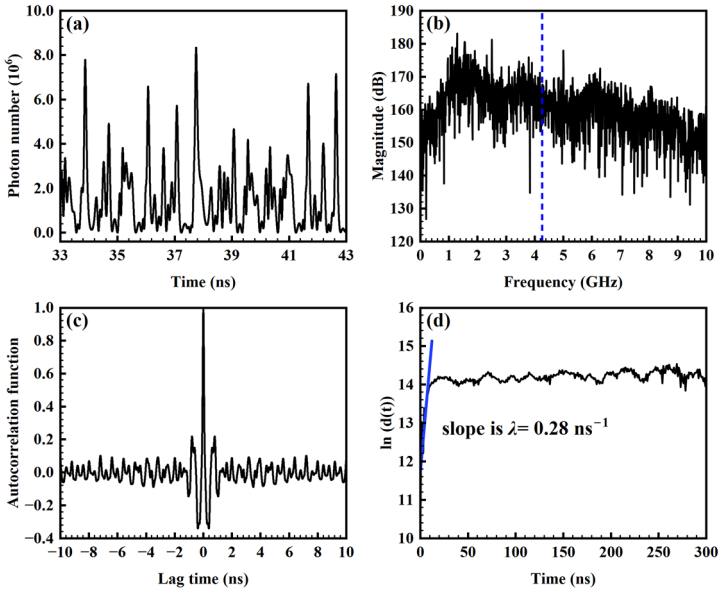

Figure 8. The nonlinear dynamics of the ICL with modulated optical injection. The injection ratio is fixed at −5 dB, and the detuning frequency is −5.75 GHz. (**a**) time series, (**b**) RF spectrum, (**c**) autocorrelation functions, (**d**) the largest Lyapunov exponent. The bias currents of master and slave lasers in the simulation are 1.2I_{th}. The modulation frequency and the modulation depth of the master laser are set to be 2.5 GHz and 0.65, respectively.

In addition to the 2.5 GHz modulation frequency case, we found that when the modulation frequency is 2 GHz, and the bias current is 1.2I_{th}, a 4.01 GHz bandwidth chaos can also be obtained, where the frequency detuning is −4 GHz, modulation depth is 0.15, and injection ratio is −10 dB. We notice that under modulated optical injection, frequency detuning in the range of −6 GHz to 6 GHz, relatively high-frequency detuning helps enlarge the bandwidth of chaos. For a fixed optical injection, relatively high-frequency detuning induces stable high-frequency period-1 oscillations, as shown in Figure 4b,c.

Further, we explore the influence of a relatively high bias current of 2I_{th} on the chaos bandwidth. Higher bias currents introduce high-frequency responses, as shown in Figure 2. Here, the modulation frequency and the modulation depth are respectively set at 5 GHz and 0.3 for 2I_{th}. Figure 9 shows the output state map of the slave laser under modulated optical injection. It is found that for a bias current at 2I_{th}, chaos arises in modulated optical injection. As such, we can obtain chaos of 6.00 GHz bandwidth when the bias current of master and slave laser at 2I_{th}, modulation frequency and modulation depth are respectively 5 GHz and 0.3, the detuning frequency is −3.75 GHz, and the injection ratio is −9 dB. When we set the detuning frequency at −6 GHz and the injection ratio at −5 dB, the bandwidth of chaos is enhanced to 7.00 GHz. It can be anticipated that

an exhaustive exploration of the effect of varying the experimentally controllable parameters would demonstrate other combinations of these parameters, which would yield similar chaos bandwidths.

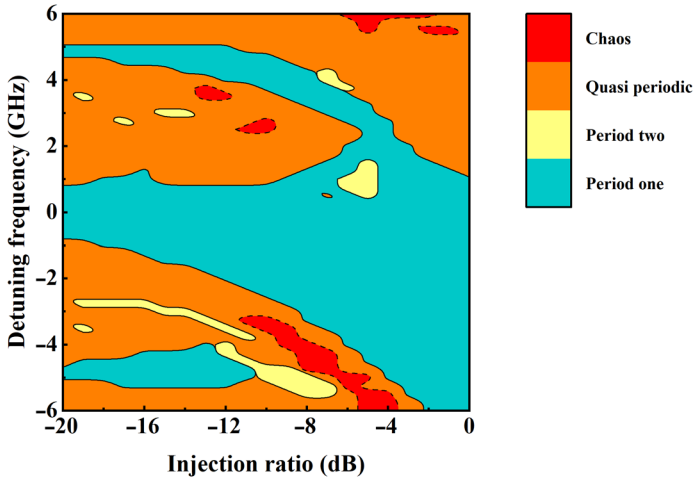

Figure 9. Detuning versus injection strength map of the nonlinear dynamics of the slave ICL with modulated optical injection. The bias currents of the master and slave lasers in the simulation are $2I_{th}$. The modulation frequency and the modulation depth of the master laser are set as 5 GHz and 0.3.

As it is found that a relatively high bias current introduces broader bandwidth chaos, we further increase the bias current to $3I_{th}$, where 8.56 GHz chaos bandwidth is obtained when the modulation frequency and modulation depth are respectively 7.5 GHz and 0.4. The bandwidth of chaos can be further enhanced by increasing the bias current to $4I_{th}$, with modulation frequencies in the range of 4 GHz to 10 GHz, as presented in Figure 10a. Figure 10b displays the corresponding modulation depths. In accordance with Figure 2, the peak-to-peak amplitude increases as the modulation frequency increases until the modulation frequency approaches the relaxation frequency of the ICL and then decreases as the modulation frequency increases further. In order to generate broadband chaos, a deep modulation depth is needed when the modulation frequency approaches the 3 dB bandwidth of the device. 10.04 GHz bandwidth chaos is generated when the bias current is $4I_{th}$, with a modulation frequency of 9.5 GHz and modulation depth of 0.85, as shown in Figure 10. It has been pointed out that using a bias current four times the threshold is close to the limit of experimentally demonstrated ICLs [35,36]. Therefore, further increasing the bias current to enlarge the bandwidth of chaos would be challenging.

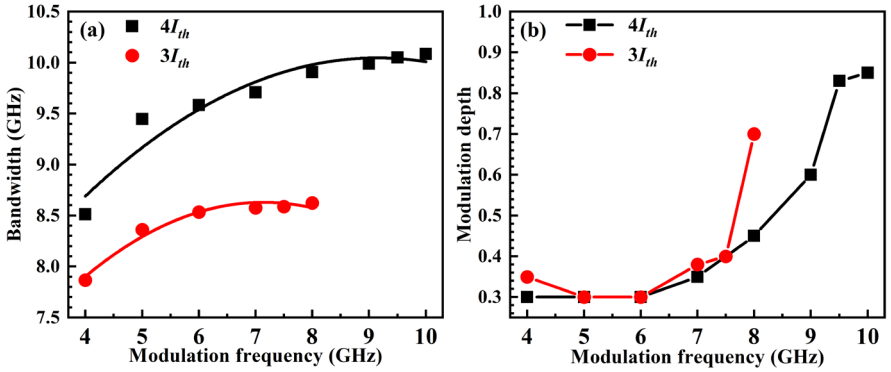

Figure 10. (**a**) Chaos bandwidth as a function of modulation frequency and (**b**) the required modulation depth, where bias currents are $3I_{th}$ (red circles) and $4I_{th}$ (black squares).

The above results are obtained for the case when the gain stage number m is 10. In ref. [17] we showed that the gain stage number also affects the chaos bandwidth. Thus, we increase the stage number from 10 to 17 to examine the enhancement of chaos bandwidth while setting the bias current at $3I_{th}$ to ensure practical operation. Figure 11 shows the bandwidth of chaos as a function of the ICL stage number. When the stage number is 17, a 10.11 GHz chaos bandwidth is attained, as seen in Figure 11. The insets of Figure 10 respectively show the RF spectrum (Figure 11a) and time series (Figure 11b) for m = 17. We also find that when the stage number is increased to 20, and the modulation frequency and the modulation depth, respectively, set at 8 GHz and 0.7, the bandwidth of mid-infrared chaos reaches 11.58 GHz.

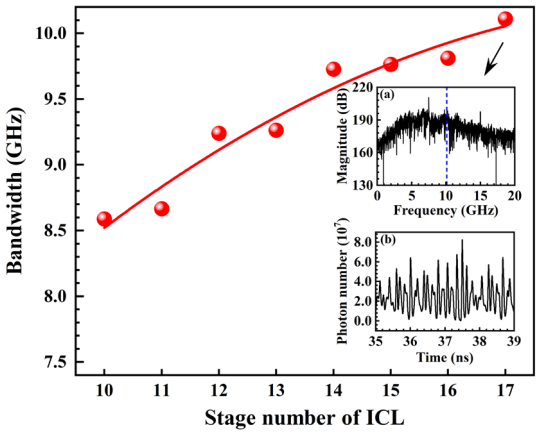

Figure 11. Bandwidth of chaos as a function of ICL staged-number with bias current $3I_{th}$, modulation frequency 7.5 GHz and modulation depth 0.4. The insets show the (**a**) RF spectrum and (**b**) time series for m = 17.

4. Conclusions

In this paper, we have simulated the nonlinear dynamics of ICLs subject to both steady-state and amplitude-modulated optical injection. Using different modulation depths, the output of the ICL under amplitude-modulated optical injection displays multi-periodic dynamics or chaos, which replaces period-1 oscillations or a stable locking state for fixed optical injection. In order to generate 10 GHz broad-bandwidth chaos, relatively large bias currents, high modulation frequency, and modulation depth are necessary; an increased gain stage number is also required. The results reported here have taken into account the practical limitations of the bias current, which may be safely applied to state-of-the-art ICLs. Nevertheless, the results obtained provide strong motivation for pursuing this approach to provide multi-Gbit/s to 10-Gbit/s long-distance secure optical communication in free space, as well as offering millimeter-range resolution for remote chaotic lidar.

Author Contributions: Conceptualization, H.H. and K.A.S.; methodology, J.Z. and K.A.S.; software, J.X. and M.H.; validation, H.H.; formal analysis, J.X. and M.H.; investigation, H.H. and J.X.; resources, H.H., Z.J., and J.Z.; data curation, J.X.; writing—original draft preparation, H.H. and J.X.; writing—review and editing, H.H. and K.A.S.; visualization, J.X.; supervision, H.H.; project administration, H.H.; funding acquisition, H.H., Z.J., and J.Z. All authors have read and agreed to the published version of the manuscript.

Funding: This research was funded by the Fundamental Research Program of Shanxi Province, grant numbers (20210302123185, 202103021224038 and 202203021221079), and the Research Project Supported by Shanxi Scholarship Council of China (2021-032), and the National Natural Science

Foundation of China (61741512), and the Fund for Shanxi "1331 Project" Key Innovative Research Team.

Institutional Review Board Statement: Not applicable.

Informed Consent Statement: Not applicable.

Data Availability Statement: The data presented in this study are available upon request from the corresponding author.

Conflicts of Interest: The authors declare no conflicts of interest.

Abbreviations

The following abbreviations are used in this manuscript:

ICL	interband cascade laser
ICLs	interband cascade lasers
QCLs	quantum cascade lasers
DFB	distributed feedback
VCSELs	vertical-cavity surface-emitting lasers
SWG	sinusoidal waveform generator
BS	beam splitter
RF	radio frequency

References

1. Spitz, O.; Herdt, A.; Wu, J.; Maisons, G.; Carras, M.; Wong, C.-W.; Elsäßer, W.; Grillot, F. Private communication with quantum cascade laser photonic chaos. *Nat. Commun*. **2021**, *12*, 3327.
2. Soibel, A.; Wright, M.W.; Farr, W.H.; Keo, S.A.; Hill, C.J.; Yang, R.Q. Midinfrared interband cascade laser for free space optical communication. *IEEE Photonics Technol. Lett*. **2010**, *22*, 121–123.
3. Ohtsubo, J. *Semiconductor Laser Stability, Instability and Chaos Second*, Enlarged Edition; Springer Series in Optical Sciences; Springer: Cham, Switzerland, 2008; Volume 111.
4. Lin, F.Y.; Liu, J.M. Chaotic lidar. *IEEE J. Sel. Top. Quantum Electron*. **2004**, *10*, 991–997.
5. Sciamanna, M.; Shore, K.A. Physics and applications of laser diode chaos. *Nat. Photonics* **2015**, *9*, 151–162.
6. Han, H.; Xu, J.D.; Cheng, X.M.; Jia, Z.W.; Zhang, J.G.; Shore, K.A. Simulation of Gb/s free space optical secure communication using interband cascade laser chaos. *Opt. Commun*. **2024**, *221*, 130424.
7. Wang, L.S.; Guo, Y.Y.; Li, P.; Zhao, T.; Wang, Y.C.; Wang, A.B. White-chaos radar with enhanced range resolution and anti-jamming capability. *IEEE Photonics Technol. Lett*. **2017**, *29*, 1723–1726.
8. Wang, A.B.; Yang, Y.B.; Wang, B.J.; Zhang, B.B.; Li, L.; Wang, Y.C. Generation of wideband chaos with suppressed time-delay signature by delayed self-interference. *Opt. Express* **2013**, *21*, 8701–8710.
9. Han, H.; Zhang, M.J.; Shore, K.A. Chaos bandwidth enhancement of Fabry–Pérot laser diode with dual-mode continuous-wave optical injection. *IEEE J. Quantum. Electron*. **2019**, *55*, 2000708.
10. Zhao, A.K.; Jiang, N.; Zhang, Y.Q.; Peng, J.F.; Liu, S.Q.; Qiu, K. Semiconductor laser-based multi-channel wideband chaos generation using optoelectronic hybrid feedback and parallel filtering. *J. Light. Technol*. **2022**, *40*, 751–761.
11. Spitz, O.; Wu, J.G.; Herdt, A.; Carras, M.; Elsäßer, W.; Wong, C.-W. Investigation of chaotic and spiking dynamics in mid-infrared quantum cascade lasers operating continuous-waves and under current modulation. *IEEE J. Sel. Top. Quantum Electron*. **2019**, *25*, 1200311.
12. Jumpertz, L.; Schires, K.; Carras, M.; Sciamanna, M.; Grillot, F. Chaotic light at mid-infrared wavelength. *Light Sci. Appl*. **2016**, *5*, e16088.
13. Peng, Y.-B.; Zhao, B.-B.; Wang, C. Nonlinear dynamics of a quantum cascade laser with optical injection. *Opt. Express* **2022**, *30*, 27593–27601.
14. Peng, Y.B.; Liu, S.; Kovanis, V.; Wang, C. Uniform spike trains in optically injected quantum cascade oscillators. *Chaos* **2023**, *33*, 123127.
15. Vurgaftman, I.; Bewley, W.W.; Canedy, C.L.; Kim, C.S.; Kim, M.; Lindle, J.R.; Merritt, C.D.; Abell, J.; Meyer, J.R. Mid-IR type-II interband cascade lasers. *IEEE J. Sel. Top. Quantum Electron*. **2011**, *17*, 1435–1444.
16. Deng, Y.; Zhao, B.-B.; Wang, C. Linewidth broadening factor of an interband cascade laser. *Appl. Phys. Lett*. **2019**, *115*, 181101.

17. Han, H.; Cheng, X.M.; Jia, Z.W.; Shore, K.A. Nonlinear dynamics of interband cascade laser subjected to optical feedback. *Photonics* **2021**, *8*, 366.
18. Deng, Y.; Zhao, Z.-F.; Zhao, B.-B.; Wang, X.-G.; Zhao, S.Y.; Wu, J.G.; Grillot, F.; Wang, C. Mid-infrared hyperchaos of interband cascade lasers. *Light Sci. Appl*. **2022**, *11*, 7.
19. Peng, Y.B.; Dai, Z.C.; Lin, K.L.; Wang, P.-L.; Shen, Z.J.; Chen, B.L.; Grillot, F.; Wang, C. Broadband chaos of an interband cascade laser with a 6-GHz bandwidth. *Opt. Lett*. **2024**, *49*, 3142–3145.
20. Liu, J.; Wu, Z.; Zhao, M.; Yang, K.; Liu, S.M.; Liu, J.Q.; Xia, G.Q. Low-frequency regular pulse and intermittent oscillation in a mid-infrared interband cascade laser with optoelectronic feedback. *Opt. Express* **2023**, *31*, 29012–29018.
21. Lin, K.L.; Wang, P.L.; Peng, Y.B.; Deng, Y.; Wang, C. Nonlinear dynamics of an interband cascade laser with optical injection. *Opt. Express* **2024**, *32*, 16722–16731.
22. Desmet, R.; Virte, M. Laser diodes with modulated optical injection: Towards a simple signal processing unit? *J. Phys. Photonics* **2020**, *2*, 025002.
23. Li, N.Q.; Nguimdo, R.M.; Locquet, A.; Citrin, D.S. Enhancing optical-feedback-induced chaotic dynamics in semiconductor ring lasers via optical injection. *Nonlinear Dyn*. **2018**, *92*, 315–324.
24. Wu, J.C.; Zeng, Y.; Zhou, P.; Li, N.Q. Broadband chaos generation in VCSELs with intensity-modulated optical injection. *Opt. Laser Technol*. **2023**, *159*, 108994.
25. Lang, R.; Kobayashi, K. External optical feedback effects on semiconductor injection laser properties. *IEEE J. Quantum. Electron*. **1980**, *16*, 347–355.
26. Deng, Y.; Wang, C. Rate equation modeling of interband cascade lasers on modulation and noise dynamics. *IEEE J. Quantum. Electron.* **2020**, *56*, 2300109.
27. Shi, Z.X.; Zhao, T.; Wang, Y.C.; Wang, A.B. High-sensitivity fiber fault detection method using feedback-delay signature of a modulated semiconductor laser. *Photonics* **2022**, *9*, 454.
28. Vurgaftman, I.; Canedy, C.L.; Kim, C.S.; Kim, M.; Bewley, W.W.; Lindle, J.R.; Abell, J.; Meyer, J.R. Mid-infrared interband cascade lasers operating at ambient temperatures. *New J. Phys.* **2009**, *11*, 125015.
29. Bewley, W.W.; Lindle, J.R.; Kim, C.S.; Kim, M.; Canedy, C.L.; Vurgaftman, I.; Meyer, J.R. Lifetimes and Auger coefficients in type-II W interband cascade lasers. *Appl. Phys. Lett*. **2008**, *93*, 041118.
30. Yang, R.Q. Mid-infrared interband cascade lasers based on type-II heterostructures. *Microelectron. J.* **1999**, *30*, 1043–1056.
31. Coldren, L.A.; Corzine, S.W.; Mašanović, M.L. *Diode Lasers and Photonic Integrated Circuits*, 2nd ed.; John Wiley & Sons, Inc.: Hoboken, NJ, USA, 2012.
32. Fan, J.F.; Deng, Y.; Ning, C.; Liu, S.M.; Wang, C. Differential gain and gain comperssion of an overdamped interband cascade laser. *Appl. Phys. Lett*. **2021**, *119*, 081101.
33. Lin, F.Y.; Chao, Y.-K.; Wu, T.C. Effective bandwidths of broadband chaotic signals. *IEEE J. Quantum Electron*. **2012**, *48*, 1010–1014.
34. Kantz, H.; Schreiber, T. *Nonlinear Time Series Analysis*; Cambridge University Press: Cambridge, UK, 1997.
35. Kim, C.S.; Kim, M.; Abell, J.; Bewley, W.W.; Merritt, C.D.; Canedy, C.L.; Vurgaftman, I.; Meyer, J.R. Mid-infrared distributed-feedback interband cascade lasers with continuous-wave singlemode emission to 80 °C. *Appl. Phys. Lett*. **2012**, *101*, 061104.
36. Xie, F.; Stocker, M.; Pham, J.; Towner, F.; Shen, K.; Wang, J.; Lascola, K. Distributed feedback interband cascade lasers with top grating and corrugated sidewalls. *Appl. Phys. Lett*. **2018**, *112*, 131102.